

Radial k-t FOCUSS for High-Resolution Cardiac Cine MRI

Hong Jung,¹ Jaeseok Park,² Jaeheung Yoo,³ and Jong Chul Ye^{1*}

A compressed sensing dynamic MR technique called k-t FOCUSS (k-t FOcal Underdetermined System Solver) has been recently proposed. It outperforms the conventional k-t BLAST/SENSE (Broad-use Linear Acquisition Speed-up Technique/SENSitivity Encoding) technique by exploiting the sparsity of x-f signals. This paper applies this idea to radial trajectories for high-resolution cardiac cine imaging. Radial trajectories are more suitable for high-resolution dynamic MRI than Cartesian trajectories since there is smaller tradeoff between spatial resolution and number of views if streaking artifacts due to limited views can be resolved. As shown for Cartesian trajectories, k-t FOCUSS algorithm efficiently removes artifacts while preserving high temporal resolution. k-t FOCUSS algorithm applied to radial trajectories is expected to enhance dynamic MRI quality. Rather than using an explicit gridding method, which transforms radial k-space sampling data to Cartesian grid prior to applying k-t FOCUSS algorithms, we use implicit gridding during FOCUSS iterations to prevent k-space sampling errors from being propagated. In addition, motion estimation and motion compensation after the first FOCUSS iteration were used to further sparsify the residual image. By applying an additional k-t FOCUSS step to the residual image, improved resolution was achieved. In vivo experimental results show that this new method can provide high spatiotemporal resolution even from a very limited radial data set. Magn Reson Med 63:68–78, 2010. © 2009 Wiley-Liss, Inc.

Key words: radial trajectory; dynamic MR imaging; gridding method; FOCUSS; motion estimation and motion compensation; residual encoding

Cardiac cine MRI requires high-speed data acquisition to maximize spatiotemporal resolution while reducing breath-hold times for patients. For studies of left ventricular functions, an in-plane spatial resolution of 2–2.5 mm is usually used. Higher resolutions up to 1–2 mm are often required to study finer structures, such as cardiac valves and patent foramen ovale (1). Typical imaging field of view (FOV) for cardiac MR studies is about $250 \times 250 \text{ mm}^2$. Therefore, to cover the entire volume of a heart, standard matrix sizes of 100×256 and higher resolution matrix sizes of 192×256 are used to meet resolution requirements (1).

These resolution requirements are demanding, even for ultrafast pulse sequence, such as balanced steady-state free precession (bSSFP) which is a standard pulse sequence for cardiovascular MRI due to its ability to achieve high signal-to-noise ratios and high contrast-to-noise ratios between myocardium and blood (2). To minimize the total number of heartbeats in electrocardiogram gating while maintaining high spatiotemporal resolution, undersampled radial trajectories have been investigated as an alternative (3). Radial trajectories have several advantages over Cartesian trajectories for dynamic MRI. In contrast to Cartesian trajectories, spatial resolution in radial trajectories is mainly determined by the imaging FOV, and there is only a limited tradeoff between spatial resolution and number of views. Furthermore, due to oversampling of the central k-space region, radial trajectories are more robust to motion artifacts (3). Therefore, the combination of undersampled radial trajectories with high signal-to-noise ratio and contrast-to-noise ratio sequences like balanced steady-state free precession, for example, may be suitable for cardiac MRI. However, there still remain some image quality degradation issues related to streaking artifacts for the case of high acceleration factor. Consider a typical pulse repetition time of 4 ms. A simple calculation shows that acquisition of an entire volume using eight slices within a single breath hold (about 16 sec) only allows times for about 32 radial lines per each cardiac phase. This results in severe undersampling streak artifacts, which should be resolved for routine use employing radial acquisition.

Recently, several novel approaches have been developed to reduce acquisition time for cardiac cine. For example, parallel imaging method such as sensitivity encoding (SENSE) (4), simultaneous acquisition of spatial harmonics (SMASH) (5), and generalized autocalibrating partial parallel acquisition (GRAPPA) (6) have been developed by exploiting coil sensitivity diversity. In contrast, temporal filtering approaches such as unaliasing by Fourier encoding the overlaps using the temporal dimension (UNFOLD) (7) and time adaptive sensitive encoding (TSENSE) (8) exploit the temporal redundancy in cardiac sequences. Another breakthrough is a model-based approach called k-t BLAST/SENSE (9). With additional information acquired during the training phase, k-t BLAST/SENSE reconstructs images from undersampled acquisition data. In radial acquisition, the oversampled center k-space region of radial trajectory usually provides low-resolution images required for k-t BLAST/SENSE. These low-resolution images eliminate the necessity of a training phase in k-t BLAST/SENSE.

Another recent development in dynamic MRI is the introduction of the so-called compressed sensing theory (10–13) borrowed from the signal processing community. According to this theory, perfect reconstruction is possible even from data taken at sampling rates dramatically lower than the Nyquist sampling limit. This is achieved by solving an l_1 minimization problem, when the nonzero spectral signal

¹Bio-Imaging and Signal Processing Laboratory, Department of Bio and Brain Engineering, Korea Advanced Institute of Science and Technology (KAIST), Republic of Korea

²Department of Radiology and Research Institute of Radiological Science, Yonsei University College of Medicine, Seoul, Republic of Korea

³ Medison Co., Ltd., Seoul, Republic of Korea

Grant sponsor: Korea Research Foundation; Grant number: KRF-2007-313-D00593.

Grant sponsor: Korea Science and Engineering Foundation; Grant number: 2009-0081089.

*Correspondence to: Jong Chul Ye, Ph.D., Department of Bio and Brain Engineering, KAIST, 373-1 Guseong-dong Yuseong-gu, Daejeon 305-701, Korea. E-mail: jong.ye@kaist.ac.kr

Received 14 January 2009; revised 10 July 2009; accepted 17 July 2009.

DOI 10.1002/mrm.22172

Published online 26 October 2009 in Wiley InterScience (www.interscience.wiley.com).

© 2009 Wiley-Liss, Inc.

is sparse and the samples are obtained using an *incoherent* basis (14). Recently, we have uncovered an intriguing link between the compressed sensing and k-t BLAST/SENSE by considering that k-t BLAST/SENSE corresponds to the first iteration of our compressed sensing algorithm called k-t FOCUSS (11,12). Furthermore, we demonstrated that motion estimation and compensation (ME/MC) after the first application of k-t FOCUSS can significantly sparsify the residual signal. After ME/MC, additional applications of k-t FOCUSS effectively encode the remaining residual signals (12).

The main contribution of this paper is to extend k-t FOCUSS algorithm to radial trajectories to achieve high spatiotemporal resolutions in cardiac cine imaging. In particular, in order to reduce computational burden and prevent error propagation during gridding, we developed an *implicit* gridding method where the radial data are transformed to and from a Cartesian grid during the FOCUSS iterations. Similar to Cartesian k-t FOCUSS, after the initial application of FOCUSS, ME/MC (15) using a high-resolution reference frame was applied to the image domain to sparsify the residual image. Our proposed radial k-t FOCUSS is expected to yield the high spatiotemporal resolution without apparent streaking artifacts desirable for cardiac cine imaging.

THEORY

Compressed Sensing Formulation

In radial trajectory acquisition, an MR scanner acquires data on polar coordinates of k -space as follows:

$$v(R, \theta, t) = \iint \sigma(x, y, t) e^{j2\pi R(x \cos \theta + y \sin \theta)} dx dy, \quad [1]$$

where $\sigma(x, y, t)$ is the image content resulting from tissue property and sequence parameters at position (x, y) and time t , and $v(R, \theta, t)$ is the measurement on the polar coordinate (R, θ) of k -space. By exploiting the periodic motion of a moving heart, we can apply a Fourier transform in the temporal direction to make the signal sparse. In this case, Eq. [1] becomes

$$v(R, \theta, t) = \iint \rho(x, y, f) e^{j2\pi R(x \cos \theta + y \sin \theta)} e^{j2\pi ft} dx dy df, \quad [2]$$

where $\rho(x, y, f)$ is the temporal Fourier transform of $\sigma(x, y, t)$. We now write Eq. [2] in matrix form:

$$\mathbf{v} = \mathbf{M}\mathbf{F}_s\mathbf{R}\mathbf{F}_t\boldsymbol{\rho}, \quad [3]$$

where $\boldsymbol{\rho}$ represents the stacked vector of the pixel values of unknown x-f spectrum of dynamic images and \mathbf{v} represents measurements in k-t space; \mathbf{F}_t , \mathbf{R} , and \mathbf{F}_s imply a Fourier transform along the temporal direction, radon transform (projection), and one-dimensional Fourier transform along the radial direction of the sinogram, respectively. \mathbf{M} is the sampling operator on the radial trajectories in k -space. If a prediction $\boldsymbol{\rho}_0$ for $\boldsymbol{\rho}$ is available (12), we can decompose the signal $\boldsymbol{\rho} = \boldsymbol{\rho}_0 + \Delta\boldsymbol{\rho}$, where $\Delta\boldsymbol{\rho}$ denotes a residual term (12). Then, Eq. [3] can be converted into

$$\Delta\mathbf{v} \triangleq \mathbf{v} - \mathbf{M}\mathbf{F}_s\mathbf{R}\mathbf{F}_t\boldsymbol{\rho}_0 = \mathbf{M}\mathbf{F}_s\mathbf{R}\mathbf{F}_t\Delta\boldsymbol{\rho}. \quad [4]$$

To enhance temporal resolution, the number of measurements should be limited by skipping some angular sampling. However, if the number of measurements does not satisfy the Nyquist sampling limit, substantial streaking artifacts are often observed. In this paper, we solve this problem by applying compressed sensing. According to compressed sensing (14,16), very accurate signal reconstruction is possible even from very limited measurements if the signal can be represented sparsely in a modeling basis and the measurement bases are incoherent from the modeling basis. By exploiting the sparsity of the cardiac cine image in x-f space and using efficient prediction to sparsify the residual $\Delta\boldsymbol{\rho}$ (11,12), we therefore convert Eq. [4] into an l_1 minimization problem under the sparsity constraint on $\Delta\boldsymbol{\rho}$.

k-t FOCUSS was developed to address the l_1 minimization problem using a reweighted quadratic optimization technique (11,12). Accordingly, radial k-t FOCUSS is implemented to find

$$\Delta\boldsymbol{\rho}_{l+1} = \mathbf{W}_l \mathbf{q}_l, \quad [5]$$

by solving the following l_2 optimization problem.

$$\begin{aligned} & \text{minimize} \quad \|\mathbf{q}_l\|_2 \\ & \text{subject to} \quad \|\mathbf{v} - \mathbf{M}\mathbf{F}_s\mathbf{R}\mathbf{F}_t\mathbf{W}_l\mathbf{q}_l - \mathbf{M}\mathbf{F}_s\mathbf{R}\mathbf{F}_t\boldsymbol{\rho}_0\|_2 \leq \epsilon, \end{aligned} \quad [6]$$

where \mathbf{W}_l is a diagonal weighting matrix at the l -th FOCUSS update:

$$\mathbf{W}_{l+1} = \begin{pmatrix} |\Delta\rho_{l+1}(1)|^p & 0 & \dots & 0 \\ 0 & |\Delta\rho_{l+1}(2)|^p & \dots & 0 \\ \vdots & \vdots & \ddots & \vdots \\ 0 & 0 & \dots & |\Delta\rho_{l+1}(N)|^p \end{pmatrix}, \quad 1/2 \leq p \leq 1. \quad [7]$$

Radial k-t FOCUSS iteratively solves Eq. [6] and successively updates \mathbf{W}_l until the solution $\Delta\boldsymbol{\rho}_l$ converges. As previously shown (11), this algorithm solves the l_1 minimization problem by setting $p = 0.5$.

Usually, projection and back-projection operations come with heavy computational cost. To resolve this issue, we used an implicit gridding method that replaces projection and back-projection. We combine this gridding operation into the radial k-t FOCUSS iteration. Specifically, Eq. [6] is modified as follows:

$$\begin{aligned} & \text{minimize} \quad \|\mathbf{q}_l\|_2 \\ & \text{subject to} \quad \|\mathbf{v} - \mathbf{M}\mathbf{S}\mathbf{F}_x\mathbf{F}_y\mathbf{F}_t\mathbf{W}_l\mathbf{q}_l - \mathbf{F}\boldsymbol{\rho}_0\|_2 \leq \epsilon, \end{aligned} \quad [8]$$

where \mathbf{F}_x and \mathbf{F}_y are the Fourier transform along x-direction and y-direction, respectively, and \mathbf{S} is the resampling operator. Compared to Eq. [6], the relation in Eq. [8] does not include the computationally expensive projection operation. Instead, the resampling operator can be represented by

$$\bar{\mathbf{v}}_{\text{radial}} = \mathbf{S}\bar{\mathbf{v}}_{\text{cart}}, \quad [9]$$

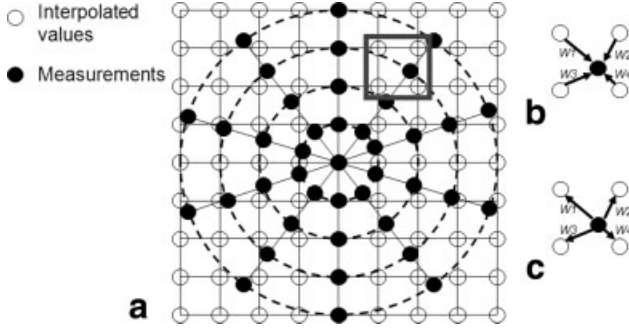


FIG. 1. (a) Radial sampling on Cartesian grid and (b) bilinear interpolation from Cartesian to polar, and (c) its adjoint operation.

where \bar{v}_{radial} and \bar{v}_{cart} are interpolated values on the radial trajectory and estimated values on the Cartesian grid, respectively (Fig. 1(a)). More specifically, if $\mathbf{V}_{\text{cart}}^j$ is a set of four neighborhoods on a Cartesian grid surrounding the j th sample in the radial trajectory $\bar{v}_{\text{radial}}^j$, then $\bar{v}_{\text{radial}}^j$ can be approximated using bilinear interpolation from the surrounding data on the Cartesian grid:

$$\bar{v}_{\text{radial}}^j = \sum_i \mathbf{w}_{(i,j)} \bar{v}_{\text{cart}}^i \quad \text{where} \quad \bar{v}_{\text{cart}}^i \in \mathbf{V}_{\text{cart}}^j, \quad [10]$$

where $\mathbf{w}_{(i,j)}$ are interpolation coefficients between the i th Cartesian data to the j th radial data, as shown in Fig. 1(b). During iterations, we require the adjoint operation \mathbf{S}^H of \mathbf{S} , which can be simply implemented (Fig. 1(c)). Specifically, let $\mathbf{V}_{\text{radial}}^j$ be a set of elements on the radial trajectory that are affected by \bar{v}_{cart}^j during a resampling operation. Then, we have

$$v_{\text{cart}}^j = \sum_i \mathbf{w}_{(j,i)} \bar{v}_{\text{radial}}^i \quad \text{where} \quad \bar{v}_{\text{radial}}^i \in \mathbf{V}_{\text{radial}}^j. \quad [11]$$

where v_{cart}^j corresponds to Cartesian data.

Prediction Using ME/MC

Recall that the $(l+1)$ -th update of our k-t FOCUSS framework can be summarized as follows:

$$\rho_{l+1} = \underbrace{\rho_0}_{\text{prediction}} + \underbrace{\Delta \rho_{l+1}}_{\text{residual encoding}}. \quad [12]$$

As demonstrated for Cartesian trajectories (12), ME/MC prediction further improves the image quality via high spatiotemporal resolution by making the residual image very sparse. Note that ME/MC is performed on the image domain. Therefore, this process can also be used for radial trajectories without concern for the differences in specific k -space trajectories.

To successfully apply ME/MC into dynamic MRI, we need at least one high-resolution reference frame. In cardiac imaging, during the diastole phase, the cardiac volume is relatively stationary. This provides an interval to acquire reference frames. Even without actual *acquisition* of high-resolution reference frames, a virtual reference frame can be obtained using temporal averaging or sliding window (SW) reconstruction (12). The main technical difficulty in using ME/MC within dynamic MRI comes from the nonexistence

of the full-resolution current frame. Recall that unlike the encoder in the video coding, the current frame σ_{cur} is unavailable in highly accelerated dynamic MRI. Here, the only available data are the reduced number of k -space data. Similar to (12), this issue can be addressed using first-pass of k-t FOCUSS before ME/MC. In this paper, for accurate ME/MC without blocking artifacts, a modified block-based ME/MC with overlapping blocks was used, as done elsewhere (12). To minimize spatial blurring due to averaging of overlapped blocks, a very small block size of 2×2 pixels is used while the total number of calculated motion vectors is equal to the total number of image pixels.

While ME/MC can efficiently decorrelate temporal redundancies, it is computationally expensive. This problem may be lessened somewhat since hardware-implemented ME/MC is already commercially available. For software implementation, various fast search methods such as three-step search (17), four-step search (18), and diamond search (19), and adaptive rood pattern search (20) have been proposed. This paper employs the adaptive rood pattern search, which significantly reduces searching steps and increases accuracy compared with other methods.

Residual Encoding

So far, we have addressed accurate prediction using ME/MC. Now, our goal is to reconstruct residual images. Recall that the updated estimate at $(l+1)$ -th iteration can be derived from Eq. [8] as follows:

$$\begin{aligned} \rho_{l+1} &= \rho_0 + \Delta \rho_{l+1} \\ &= \rho_0 + \Theta_l \hat{\mathbf{F}}^H (\hat{\mathbf{F}} \Theta_l \hat{\mathbf{F}}^H + \lambda \mathbf{I})^{-1} (\mathbf{v} - \mathbf{F} \rho_0), \quad [13] \end{aligned}$$

where $\mathbf{F} = \mathbf{M} \mathbf{F}_s \mathbf{R} \mathbf{F}_t$, $\hat{\mathbf{F}} = \mathbf{M} \mathbf{S} \mathbf{F}_x \mathbf{F}_y \mathbf{F}_t$, and $\Theta_l = \mathbf{W}_l \mathbf{W}_l^H$, respectively.

From Eq. [13], two important issues must be addressed for successful implementation of our algorithm. One is that the predicted image ρ_0 should be transformed to k -data on radial trajectories using $\mathbf{F} \rho_0$ rather than $\hat{\mathbf{F}} \rho_0$. Figure 2 (a) demonstrates this need. Suppose we have acquired fully sampled k -data on radial trajectories. Then, using filtered back-projection from sinograms, we can obtain a high-resolution reference frame. If we assume this image to be ground truth, the k -space data from the reference image should be equal to the measurement \mathbf{v} . Otherwise, the residual encoding will induce artifacts. In Fig. 2 (a), both sinograms obtained from projection and bilinear interpolation appear similar; however, the difference error clearly shows that bilinear interpolation generates more substantial error. This error is mainly due to nonuniform sampling that has more dense samples on the low frequency of k -space. Therefore, we should calculate the residual measurements using the $\mathbf{F} \rho_0$ using projection operation that is optimal for radial sampling pattern.

Another important issue is that the predicted image ρ_0 using ME/MC has different artifact patterns compared to the reconstruction using k -space data. For example, the reconstruction from radial k -space sampling patterns exhibits streaking artifacts, whereas the motion-compensated images are prone to blocking artifacts. Therefore, when reconstruction from fully sampled radial trajectories is used to calculate the mean square error (MSE)

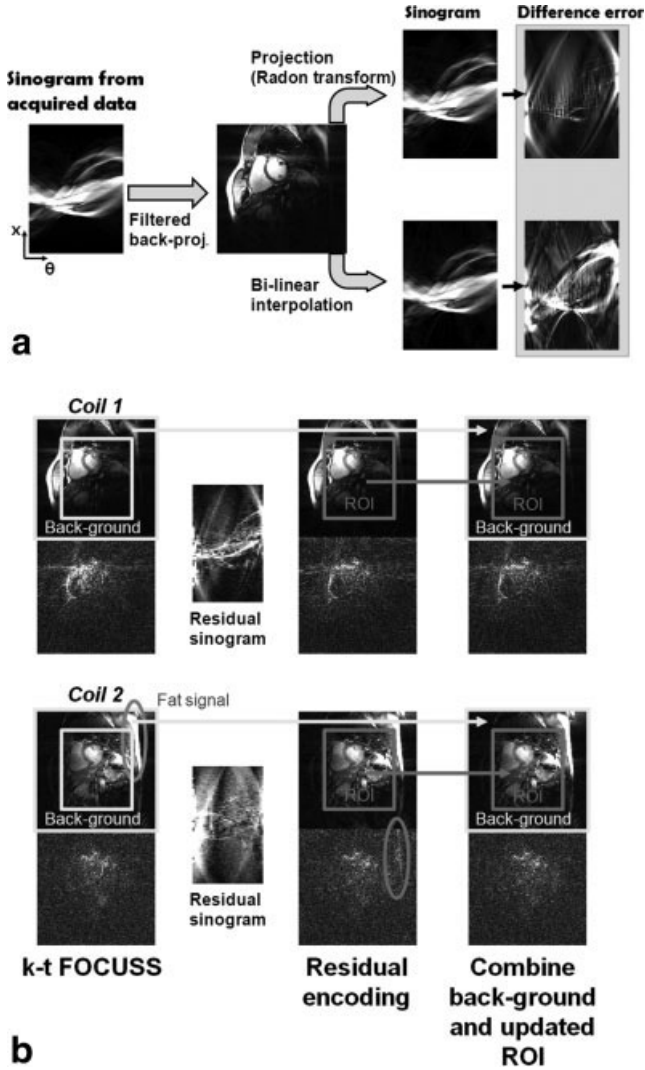


FIG. 2. (a) Comparison between $F\rho_0$ and $\hat{F}\rho_0$ in calculating residual sinogram measurement. As shown in difference error images, $F\rho_0$ is much more accurate than $\hat{F}\rho_0$. (b) If some parts are significantly bright in static image, the residual sinogram shows quite a significant signal over whole space as shown in coil 2. To overcome this, we combine ROI region from k-t FOCUSS with ME/MC and a background image from k-t FOCUSS without ME/MC.

of reconstruction, the MSE value for ME/MC is often high even though visual quality is good. This artifact is not a problem in practice, but in quantitative comparison it may lead to erroneous conclusions. This artifact can be easily remedied if we replace ρ_0 by $F_t^H \mathbf{B} \mathbf{R} F_t \rho_0$, where F_t , \mathbf{B} , and \mathbf{R} correspond to a Fourier transform along temporal direction, filtered back-projection, and radon transform, respectively. Mathematically, the operation $F_t^H \mathbf{B} \mathbf{R} F_t$ corresponds to a projection operation to the space spanned by radial k -space trajectories. Hence, by applying projection of motion-compensated ρ_0 onto this space, the artifact patterns become consistent with that of radial sampling pattern. The erroneous MSE value can then be corrected.

After the residual measurements and prediction terms are corrected, residual encoding can be performed as discussed in Section Compressed Sensing Formulation. However, unlike Cartesian k-t FOCUSS (11), we have

observed important artifacts in residual encoding (Fig. 2b). k-t FOCUSS results from coil 1 and coil 2 are displayed in the leftmost column in that figure, along with their difference images. The corresponding residual sinogram data are also illustrated for each coil. For coil 1, the residual sinogram is mostly small on overall space. However, for coil 2, relatively high residual signals are observed over the whole space. Note that coil 2 has more sensitivity in relatively static areas that contain fat signals. Hence, the residual signals are still significant for low-frequency k -space data. In order to overcome this problem, we combine the relatively static area (background) from k-t FOCUSS (without ME/MC) and dynamic moving area (region of interest [ROI]) from updated images using ME/MC + residual encoding. This hybrid method is robust in all the simulations that we have conducted.

MATERIALS AND METHODS

Downsampling Experiments

We acquired cardiac cine data using electrocardiogram-triggered segmented balanced steady state free precession pulse sequence with radial k -space sampling trajectories from a healthy volunteer at 3 T on a whole-body MR scanner (Magnetom Trio; Siemens Medical Solutions, Erlangen, Germany). Imaging parameters were as follows: pulse repetition time/echo time was 3.4/1.7 ms, flip angle was 40° , imaging FOV was $300 \times 300 \text{ mm}^2$, and the slice thickness was 3 mm. The number of views for each frame was 192, and the sample number along the readout direction was 384. This resulted in a 192×384 matrix. The cardiac parameters were as follows: 32 cardiac phases, eight views per segment, and 24 heartbeats. This provided $8 \times 24 = 192$ views for each frame, and the temporal resolution was $3.4 \times 8 \text{ ms} \cong 30 \text{ ms}$. The number of coils was seven.

To evaluate the performance of our algorithm, we implemented two types of k-t FOCUSS algorithms whose prediction terms were separately obtained using temporal averaging and ME/MC, respectively. We also used conventional methods, such as SW, and k-t BLAST algorithm. All algorithms used the same data set. The images obtained from an inverse radon transform of 192 views were used as reference results. Here, 16 cardiac phases among 32 phases were used in the simulation to investigate the performance of temporal down-sampling. The first and second simulations used 32 and 16 views corresponding to 6- and 12-fold acceleration, respectively. The sampling pattern for each frame was interleaved such that if the [1st, 13th, 25th, ..., 181st] views were sampled for the first frame, then the second frame contains [2nd, 14th, 26th, ..., 182nd] views.

To incorporate ME/MC into k-t FOCUSS, the first frame from fully sampled data was used as a reference frame for motion estimation. In real acquisition, this fully sampled frame can be obtained separately. This is because the reference frame does not need be consecutive with respect to dynamic frames. Furthermore, this fully sampled reference frame can be used for other purposes, namely, to improve reconstruction quality. More specifically, for k-t BLAST (9) and k-t FOCUSS for Cartesian trajectories (11), the temporal average is initially subtracted to avoid energy concentration in the temporal zero frequency. However, as in our 12-fold acceleration scenario with 16 temporal

frames, residual k -space measurements after subtracting the temporal average must be zero in some frames since some radial lines of the temporal average are identical to the radial measurements due to insufficient temporal redundancy. Therefore, additional improvements cannot be expected to those frames with any method. However, this problem can be effectively resolved while avoiding energy concentration on temporal DC frequency by subtracting the fully sampled reference frame instead of the temporal average. Note that this advantage is not obvious for low acceleration factors. However, when the acceleration factor is more than half of the total number of time frames, subtracting the reference frame is very effective. Therefore, in this paper, for 6-fold acceleration, temporal averages were initially subtracted, whereas in 12-fold acceleration experiments, a fully sampled reference frame was subtracted.

In Vivo Experiments

For in vivo experiments, cardiac cine and tagged cardiac cine data were acquired at 3 T on a whole-body MR scanner (Magnetom Trio; Siemens Medical Solutions). The detailed descriptions for the acquisition of cardiac cine and tagged cardiac cine data are as follows.

Cardiac Cine

In vivo experiments were performed on the same subject with the same imaging parameters used for full data acquisition. Thirty-two radial lines were acquired for each cardiac phase. This corresponds to 6-fold acceleration. In contrast to the previous downsampling experiments, 32

cardiac phases were used for reconstruction. The view ordering was as follows; The first frame had the [1st, 7th, 13th, . . . , 187th] views, the second frame had the [2nd, 8th, 14th, . . . , 188th] views, and so on. For ME/MC implementation, we used a reference frame obtained from the first cardiac phase of the fully sampled image used in Section Downsampling Experiments.

Tagged Cardiac Cine

Tagged cardiac cine data were acquired on the same subject to clearly see the spatial resolution of reconstructed images. The in vivo data with radial k -space sampling trajectories were acquired using electrocardiogram-triggered segmented spoiled GRE sequence with spatial modulation of magnetization tagging (21). Imaging parameters were as follows: pulse repetition time/echo time was 3.4/2.9 ms, flip angle was 10° , imaging FOV was $340 \times 340 \text{ mm}^2$, and the slice thickness was 10 mm. The number of views for each frame was 64 in accelerated acquisition (4-fold acceleration). In order to obtain the reference results, we also obtained fully sampled data with 256 views per frame. The sample number along the readout direction was 512. The cardiac parameters were as follows: 26 cardiac phases, eight views per segment, and eight heartbeats for 4-fold acceleration and 32 heartbeats for full acquisition. The number of coils was six.

EXPERIMENTAL RESULTS

Downsampling Experiments

We compared our two implementations of k -t FOCUSS with SW and k -t BLAST. In Fig. 3, reconstructed images

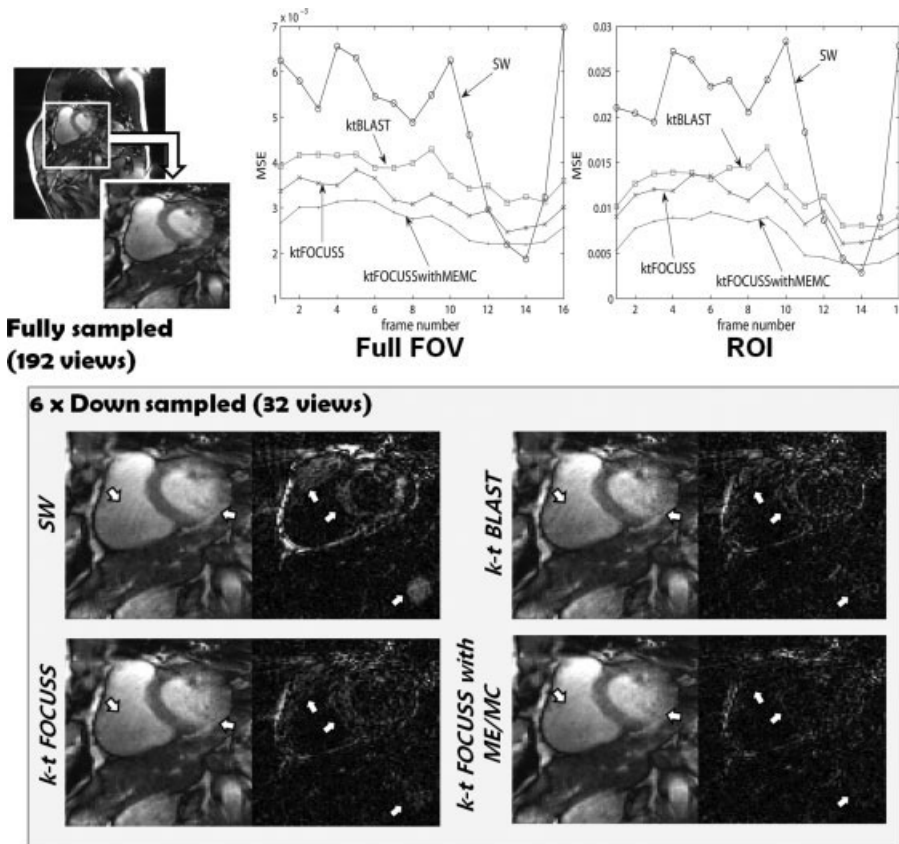


FIG. 3. Reconstruction results from SW, k -t BLAST, k -t FOCUSS, and k -t FOCUSS with ME/MC at 6-fold acceleration factor. In order to clearly show the improvements, the difference images between full-view (192 view) reconstruction and each reconstructed image are calculated. SW results in some streaking artifacts and degraded heart wall (indicated by arrows) due to temporal blurring. k -t BLAST improves temporal blurring, but there still remains streaking artifact in heart muscle. k -t FOCUSS greatly improves those problems and k -t FOCUSS with ME/MC exceeds all other methods. For quantitative analysis of errors, normalized MSEs were calculated over full FOV and ROI covering moving heart, respectively. Our algorithm shows the smallest error over most of the frames in all the cases.

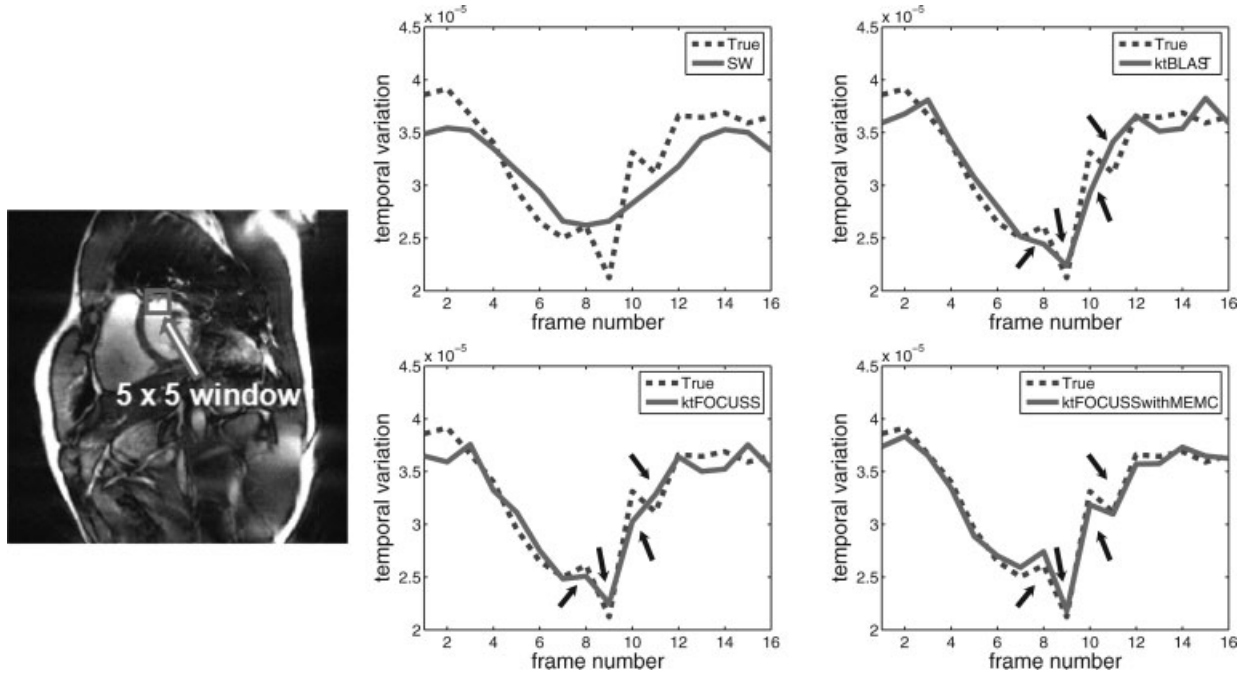


FIG. 4. The temporal variation of averaged value within the specified 5×5 pixel window is plotted for SW, k-t BLAST, k-t FOCUSS, and k-t FOCUSS with ME/MC at 6-fold down-sampling. The true variation was calculated from fully sampled reference results. In SW, detailed movements are not captured. k-t BLAST improves the movements slightly (see arrows). k-t FOCUSS further improves and k-t FOCUSS with ME/MC very closely follows true temporal variation.

from 6-fold acceleration are compared. To clearly see image quality improvements, an ROI around the heart was magnified. As indicated by the white arrows in Fig. 3, SW exhibits streaking artifacts. Furthermore, the cardiac wall was not clearly visible using SW due to temporal blurring caused by view sharing between consecutive frames. The difference error image also clearly shows temporal blurring. For k-t BLAST, the heart muscles still exhibit streaking artifacts. However, images obtained using k-t FOCUSS are much improved, and k-t FOCUSS with ME/MC outperforms all methods, without any noticeable streaking artifacts. The difference image clearly shows the improvements.

To show the improvements quantitatively, we calculated the normalized MSE within the full FOV and the ROI in Fig. 3. The normalized MSE is calculated as follows:

$$\text{normalized MSE} = \frac{\|\rho - \rho_{\text{True}}\|_2^2}{\|\rho_{\text{True}}\|_2^2}, \quad [14]$$

where ρ_{True} is the assumed reference result obtained from an inverse radon transform of 192 views. SW shows the smallest MSE between the 12th and 15th frames. Note that that period corresponds to a nearly stationary diastole phase. It was thus possible for SW to accurately reconstruct images without temporal blurring during those phases at 6-fold acceleration. For real clinical implementation, this window can be used to generate the fully sampled reference frame. Except for that period, our methods give the smallest error in both MSE plots.

For temporal resolution analysis, we plotted the temporal variation of average values within a specified 5×5 pixel window focused on the heart for each method at 6-fold acceleration (Fig. 4). The true variation was obtained

from fully sampled measurements. SW shows very blurred temporal variation. k-t BLAST improves temporal variation compared to SW, but rapidly varying components were not reproduced, as indicated by arrows. k-t FOCUSS shows better movement and k-t FOCUSS with ME/MC accurately reproduces the rapidly varying signal components.

For further analyses, we compared x-t images of the heart at a 12-fold acceleration factor (Fig. 5). As a reference result, the fully sampled image is shown at the leftmost column. As mentioned above, SW does not show any temporal variation. k-t BLAST shows some movement but some significant temporal variations were not well reproduced, as indicated by the arrows. However, k-t FOCUSS and k-t FOCUSS with ME/MC still closely follow the reference results, even for this high acceleration factor.

In Vivo Experiments

Cardiac Cine

Using 6-fold accelerated in vivo measurements, we reconstructed cine imaging using filtered back-projection, SW, k-t BLAST, k-t FOCUSS, and k-t FOCUSS with ME/MC (Fig. 6). Even though the fully sampled reference was reconstructed from separately obtained measurements, we also put that in Fig. 6 for comparison. The ROI was magnified to better see the reconstructed heart images. First, filtered back-projection shows severe streaking artifacts over the entire image. SW shows that some streaking artifacts and detailed structure, such as the anterior papillary muscle, posterior papillary muscle, and heart wall, are very blurred, as indicated by arrows. k-t BLAST reduced streaking artifacts somewhat, but detailed structures are still blurred. Finally, k-t FOCUSS and k-t FOCUSS with ME/MC very

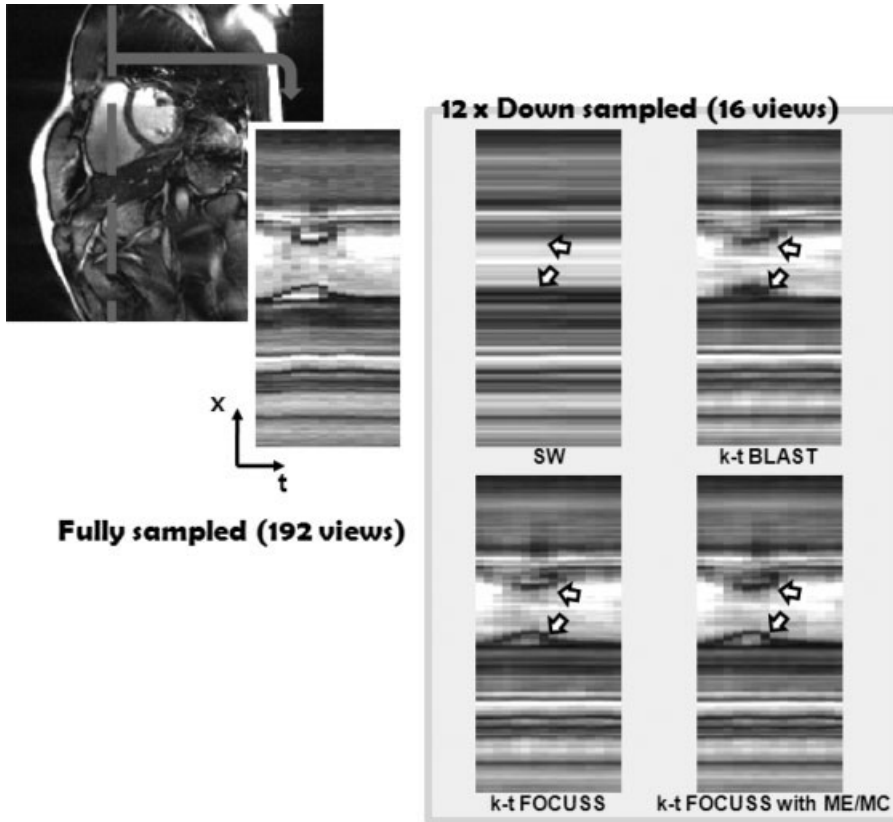


FIG. 5. For temporal resolution analysis, x-t images are illustrated. At the leftmost area, the result from fully sampled data is shown as a reference image. Using SW, k-t BLAST, k-t FOCUSS, and k-t FOCUSS with ME/MC, each result was reconstructed at 12-fold down-sampled data. The significant improvement is indicated by a white block arrow. In SW, because of serious temporal blurring, the heart movement is not reproduced at all. Even if k-t BLAST shows some movements, some important temporal variations are still missing, as indicated by arrows. Finally, k-t FOCUSS and k-t FOCUSS with ME/MC show correct heart movements.

FIG. 6. In vivo comparison of SW, k-t BLAST, k-t FOCUSS, and k-t FOCUSS with ME/MC at 6-fold acceleration. We also illustrate the fully sampled reference results the left top figure for comparison, even if this is reconstructed from a separately obtained data set. To compare the performance of each method clearly, heart regions are magnified. First, filtered back-projection shows severe streaking artifacts. SW shows some streaking artifacts and heart wall and muscles are very blurred. k-t BLAST also shows some streaking artifacts and blurred vessel. However, k-t FOCUSS and k-t FOCUSS with ME/MC show very clear texture and structures of the heart.

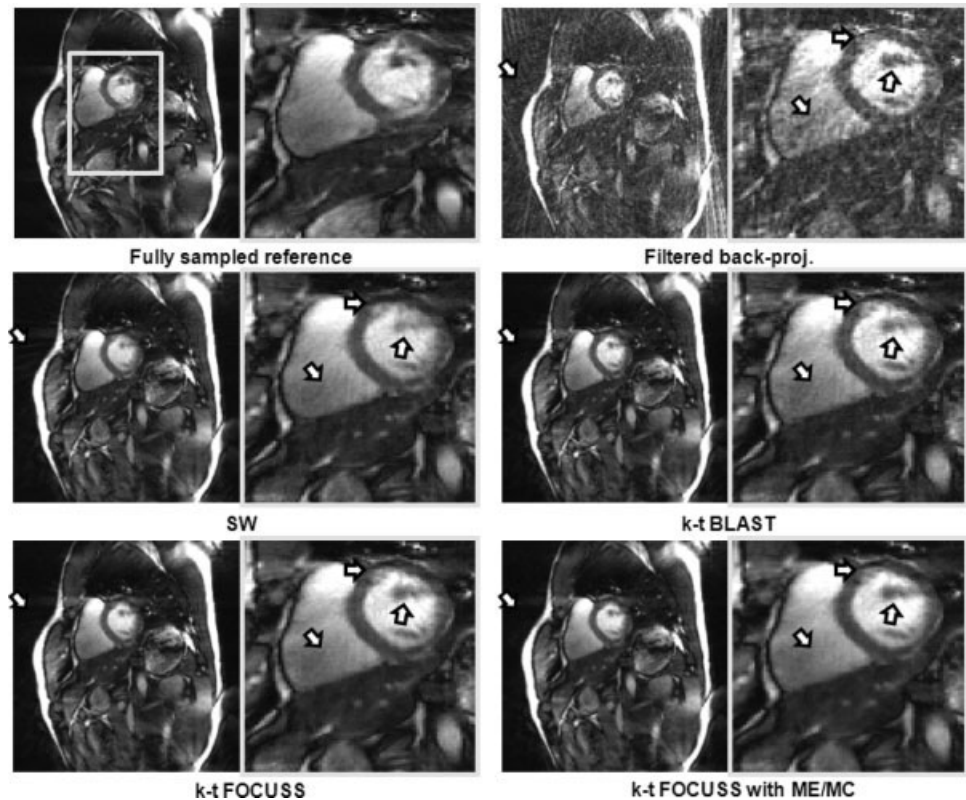
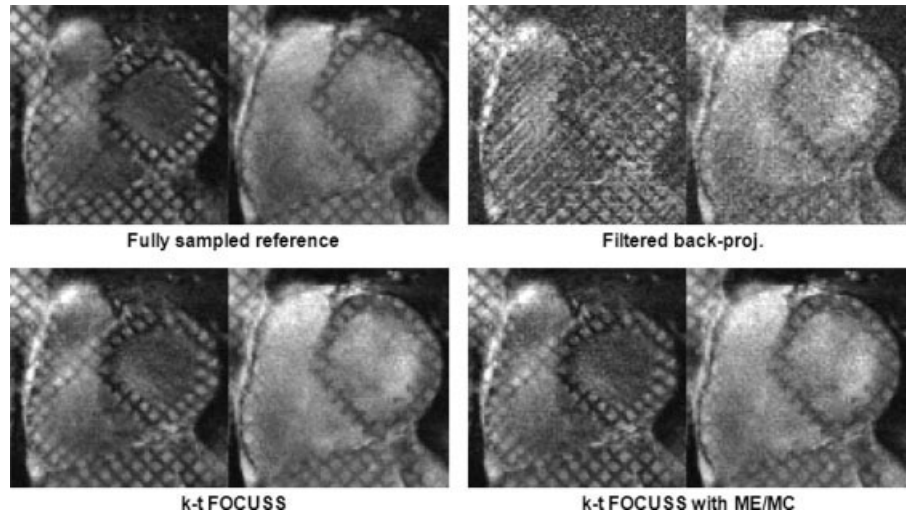


FIG. 7. In vivo cardiac MR tagging images representing systole and diastole from 4-fold acceleration. To evaluate the results of *k-t* FOCUSS and *k-t* FOCUSS with ME/MC, the fully sampled reference results are also illustrated in the left top figure. In filtered back-projection, because of overlapped gridding shape and streaking artifacts, the heart is not clearly seen. However, *k-t* FOCUSS and *k-t* FOCUSS with ME/MC accurately reconstruct heart and gridding shapes.



clearly show the heart wall and muscles while greatly suppressing streaking artifacts. Interestingly, the results of *k-t* FOCUSS and *k-t* FOCUSS with ME/MC appear to be less error prone than the fully sampled reference image around the anterior and posterior papillary muscles. This is because the fully sampled reference frame used in this work was obtained during 24 heartbeats, whereas the *k-t* FOCUSS reconstruction was obtained from four heartbeats. Hence, patient breathing artifacts were significantly reduced. This again confirms the advantage of accelerated acquisition in cardiac cine imaging.

Tagged Cardiac Cine

Tagged cine images that were reconstructed using filtered back-projection, *k-t* FOCUSS, and *k-t* FOCUSS with ME/MC from 4-fold accelerated in vivo measurements are illustrated in Fig. 7. As a reference result, we also put the fully sampled images at left top figure. In filtered back-projection, because of overlapped gridding shape and streaking artifacts, the heart is not clearly seen. However, *k-t* FOCUSS and *k-t* FOCUSS with ME/MC accurately reconstruct the heart and gridding shapes. This clearly proves the high spatial resolution of proposed methods and confirms that our methods can accurately reconstruct very sophisticated structures from limited measurements.

DISCUSSION

Accuracy of Implicit Gridding

Research focusing on gridding methods is extensive (22–26). The basic concept of gridding is to transform non-Cartesian data (such as radial trajectories) to Cartesian data. The reconstruction process can then be made much faster with the help of the fast Fourier transform. One may argue that if we could implement a perfect gridding method, *k-t* FOCUSS for Cartesian trajectory (11,12) might be simply used for radial trajectory after gridding. However, conventional gridding methods are imperfect and error prone (22–26). More specifically, they first precompensate sampled data for spatially varying densities of sampled

measurements on *k*-space, using the inverse of the sampling density. They then convolve the compensated data, using appropriate kernels, and resample onto Cartesian grids. However, finding an optimal density compensation factor for the precompensation step is nontrivial. Hence, the error in explicit gridding methods tends to propagate through iterations. This may result in severe distortion of the final reconstruction.

Compared to conventional gridding methods, we explicitly represent the resampling operator from a Cartesian grid to a radial one using bilinear interpolation within FOCUSS iterations. Gridding then becomes implicit during iterations. Such implicit gridding can prevent error propagation during iterations because the inaccuracy of approximated \mathbf{S} in Eq. [8] only affects the reconstructed image quality, rather than introducing measurement mismatch. In contrast, measurement mismatch error due to explicit gridding can be substantially amplified in the final reconstruction due to the ill-posed under sampled projection operators.

To verify the accuracy of implicit gridding, we compared its performance with that of projection/back-projection approaches without gridding using Eq [6]. Figure 8 compares the results of *k-t* FOCUSS with the implicit gridding method and projection/back-projection. The acceleration factor was 6 in both cases. Both results appear similar. However, the normalized MSE plot indicates that implicit gridding is better than projection/back-projection. Furthermore, the implicit gridding method comes with substantial gains in computational overhead compared to projection/back-projection. For example, in our experiment for 6-fold acceleration, reconstruction time using implicit gridding was about 3 min, while projection/back-projection took 22 min, for each coil reconstruction. Even if the bilinear interpolation during resampling operation looks simple, the results show that the “simple” resampling method provides more accurate results, in addition to significant time saving.

Temporal Average as a Prediction

In Section Downsampling Experiments, we briefly mentioned the drawbacks of using temporal averaging for

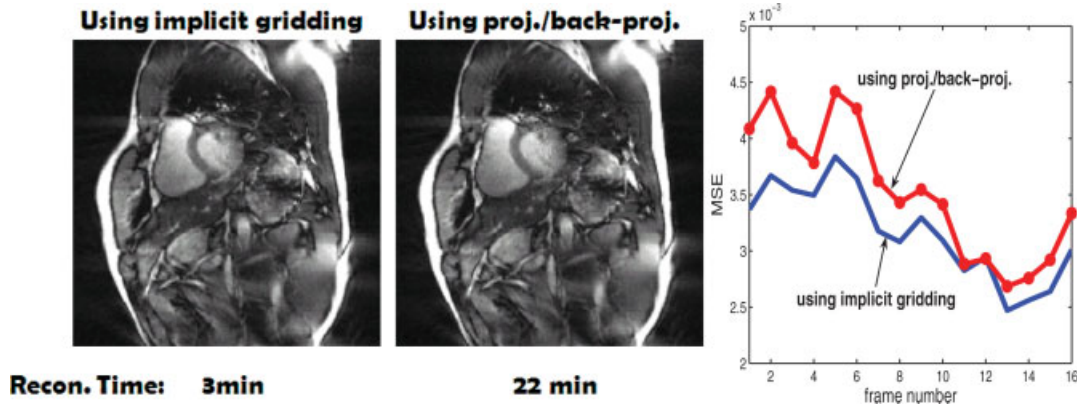


FIG. 8. The implicit gridding method within FOCUSS iteration is evaluated by comparison with projection/back-projection method within FOCUSS iteration. Actually, even though the idea to use implicit gridding algorithm started to reduce the computational burden by replacing projection and back-projection operations, the results show that implicit gridding methods not only greatly reduce required computational time but also improve reconstruction qualities.

prediction for large acceleration factors. In Fig. 9 (a), this issue is illustrated in more detail via a simple example. Here, sampling points are not repeated along the temporal direction. After subtracting the temporal average, the residual k -space data become zero so it is not possible to update results using k -t BLAST or k -t FOCUSS. In order to allow for updates, there should exist at least two views at different time frames but from the same angle. However, for very high acceleration, overlapping angle views inhibits spread of measurements in k -space, which possibly results in streaking artifacts. In order to resolve this problem, we used a fully sampled reference frame instead of temporal averaging as prediction, especially at 12-fold acceleration. Figure 9c-d show results using a fully sampled reference frame and temporal averaging, respectively, at 12-fold acceleration. The 7th and 12th frame indicate time frame corresponding to systole and diastole. To clearly show the drawbacks inherent in the use of temporal averaging for prediction, the contours of the left heart obtained from the fully sampled result (Fig. 9a) were overlaid on each image of different methods with a green line. The contours of the left heart of each resultant image were also drawn with a red line. As expected, using a reference frame as a prediction term correctly shows systole and diastole at the 7th and 12th time frame, respectively; temporal averaging as a prediction term, on the other hand, cannot represent different cardiac phases. In 6-fold acceleration where sampling points are repeated along the temporal direction, since both methods show correct cardiac phases without significant difference, we only show the result using a fully sampled reference frame in Fig. 9 (e).

Suitability of ME/MC in Dynamic MRI

For our Cartesian k -t FOCUSS implementation (12), we introduced two efficient prediction methods: two-dimensional reduced-encoding imaging by generalized-series reconstruction (12,27) and ME/MC (15). However, the application of reduced-encoding imaging by generalized-series reconstruction to radial trajectories is not well established due to the difficulty involved with generalized series representation on non-Cartesian grids. In contrast, ME/MC is still an effective prediction scheme for

non-Cartesian trajectories such as radial trajectories since all estimation and compensation are done in the image domain rather than in k -space.

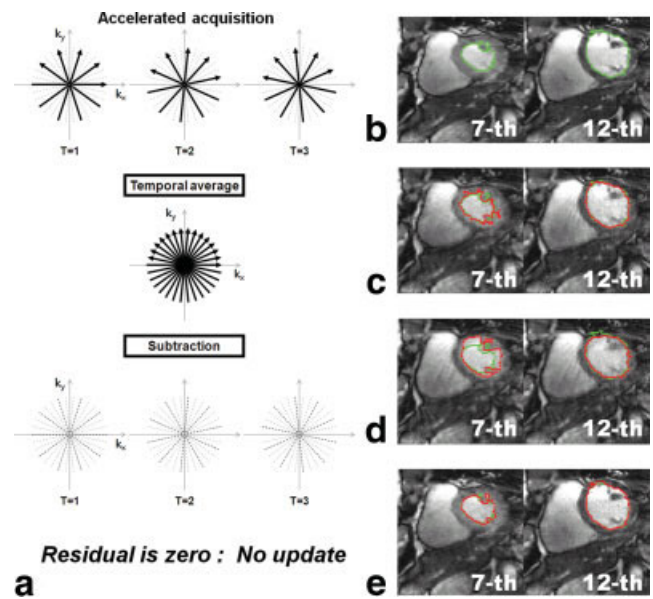


FIG. 9. (a) The case where the subtraction of temporal average results in failure of k -t FOCUSS update. In order to avoid no update, there should exist at least two same-angle views at different time frames. If that is not possible because of high acceleration, we can use a fully sampled reference frame instead of temporal average. (b-e) The results from fully sampled data, 12-fold accelerated data with a fully sampled reference frame, 12-fold accelerated data with temporal average, and 6-fold accelerated data with a fully sampled reference frame, respectively. The 7th and 12th frame indicate time frames corresponding to systole and diastole. For clear comparison, the contours of the left heart obtained from the fully sampled result and each reconstruction are overlaid on each image with green and red lines, respectively. When the acceleration factor is 12, using a fully sampled reference frame as a prediction (c) correctly shows systole and diastole, while using a temporal average as a prediction (d) cannot represent different cardiac phases. In 6-fold acceleration, both methods show correct motion, without a significant difference. To avoid image redundancy, we only included the results using a fully sampled reference frame.

Table 1
Comparison of k-t BLAST, k-t FOCUSS, and k-t FOCUSS With ME/MC in Terms of Reconstruction Time and MSE

	Reconstruction time (min)	Average MSE
k-t BLAST	1.5	0.0608
k-t FOCUSS	3	0.0512
k-t FOCUSS with ME/MC	13	0.0432

Furthermore, our ME process offers many advantages compared to its counterpart in video coding. First, the motion vectors are estimated from the data itself without additional k -space sample allocation. Therefore, a dense motion vector field, as well as multiple reference frames, can be used in the ME step to improve the estimation accuracy. Second, since no additional information is required with the more sophisticated ME/MC, a modified block-based ME/MC with overlapping blocks can be implemented to remove blocking artifacts. This overlapping ME/MC procedure with a small block size can effectively remove aliasing and streaking artifacts, as well as blocking artifacts through averaging.

Accuracy of ME/MC

In video coding where ME/MC was originally developed, various improved ME/MC methods, such as half-pel or intra/intermode block ME/MC, have been devised for improved performance. However, in contrast to video coding, which uses full-resolution current frames for ME at the encoder, in our framework, we use k-t FOCUSS reconstruction as current dynamic frames for ME. Therefore, it would be interesting to investigate whether or not half-pel or intra/intermode block ME/MC can offer improvements using our framework. Throughout extensive experiments, we observed that the sophisticated ME/MC do not provide significant improvements even with high complexity. Our ME/MC method, which uses averaging overlapped blocks and hybrid combination, appears to be optimal for most of the cases examined in this work.

Computational Complexity

Our method may appear complex because of the incorporation of ME/MC into k-t FOCUSS. Even if we already confirmed the improvement of our method compared to conventional methods including k-t BLAST, one might be curious if the improvement is enough to accept relatively large computational complexity. For clear conception, we compared k-t BLAST, k-t FOCUSS, and k-t FOCUSS with ME/MC in terms of reconstruction time and the average MSE. Reconstruction time was measured by computer CPU (central processing unit) time on a Xeon 3 GHz with 4 GB memory Linux machine using Matlab 7.0.4. The average MSE was calculated using all time frames. Table 1 compares results for one coil reconstruction. k-t FOCUSS reconstruction time was nearly double that of k-t BLAST; k-t FOCUSS is an iterative form of k-t BLAST, and two iterations are usually enough for convergence. k-t FOCUSS with ME/MC required much more time. Most of the time

was spent on ME/MC. However, since hardware implementations of ME/MC are presently available commercially, the real implementation time can be significantly reduced. Furthermore, the reconstruction step can be performed in a dedicated multiprocessor computer separated from the scanner; hence, the increase reconstruction time of 13 min does not cause delay or backlogs in workflow, which is confirmed by communications with clinicians.

Issue of Arrhythmia

Since arrhythmia often causes irregular heartbeats, the R-R peak interval in the electrocardiogram should vary between regular and arrhythmic heartbeats. Hence, cardiac phase synchronization would be more complicated. Furthermore, even in the case of tachycardia where periodic rapid heartbeats are observed, the number of cardiac phases should be significantly limited, or spatial resolution should be compromised due to the smaller number of views at each cardiac phase. Therefore, the overall performance of k-t FOCUSS might be degraded. However, we have been only dealing with healthy subjects without arrhythmia; hence, we have not observed such degradation so far.

CONCLUSION

This paper described an extension of the k-t FOCUSS algorithm to radial trajectories for high-resolution cardiac cine imaging. The implicit gridding method where radial data are transformed to Cartesian data during the FOCUSS iterations was effective in preventing error propagation and reducing computation time. To make the residual image as sparse as possible, ME/MC was used as a prediction term. This made the residual very sparse. The current dynamic frames for ME/MC were obtained through first application of k-t FOCUSS from down-sampled data. Then, using a separately obtained fully sampled reference frame and estimated current frames, ME/MC was performed. Finally, by applying an additional k-t FOCUSS step to the residual signal, high spatiotemporal images resulted. In contrast to Cartesian implementations (12), several practical issues, prompted by the irregular sampling pattern, emerged. This paper provides several remedies for this. The *in vivo* experimental results demonstrated that our new method can provide very high resolution even from very limited radial data sets.

REFERENCES

1. Lee VS. Cardiovascular MRI: physical principles to practical protocols. Philadelphia: Lippincott Williams & Wilkins; 2006.
2. Scheffler K, Lehnhardt S. Principles and applications of balanced SSFP techniques. *Euro Radiol* 2003;13:2409–2418.
3. Wild J, Paley M, Kasuboski L, Swift A, Fichelle S, Woodhouse N, Griffiths P, van Beek E. Dynamic radial projection MRI of inhaled hyperpolarized ^3He gas. *Mag Reson Med* 2003;49:991–997.
4. Pruessmann KP, Weigher M, Scheidegger MB, Boesiger P. SENSE: sensitivity encoding for fast MRI. *Magn Reson Med* 1999;42:952–962.
5. Sodickwon DK, Manning WJ. Simultaneous acquisition of spatial harmonics (SMASH): fast imaging with radiofrequency coil arrays. *Magn Reson Med* 1997;38:591–603.
6. Griswold MA, Jakob PM, Heidemann RM, Nittka M, Jellus V, Wang J, Kiefer B, Haase A. Generalized autocalibrating partially parallel acquisitions (GRAPPA). *Magn Reson Med* 2002;47:1202–1210.

7. Madore B, Glover GH, Pelc NJ. Unaliasing by Fourier-encoding the overlaps using the temporal dimension (UNFOLD), applied to cardiac imaging and fMRI. *Magn Reson Med* 1999;42:813–828.
8. Kellman P, Epstein FH, McVeigh ER. Adaptive sensitivity encoding incorporating temporal filtering (TSENSE). *Magn Reson Med* 2001;45:846–852.
9. Tsao J, Boesiger P, Pruessmann KP. k-t BLAST and k-t SENSE: Dynamic MRI with high frame rate exploiting spatiotemporal correlations. *Magn Reson Med* 2003;50:1031–1042.
10. Lustig M, Donoho D, Pauly J. Sparse MRI: the application of compressed sensing for rapid MR imaging. *Magn Reson Med* 2007;58:1182.
11. Jung H, Ye JC, Kim EY. Improved k-t BLAST and k-t SENSE using FOCUSS. *Phys Med Biol* 2007;52:3201–3226.
12. Jung H, Sung K, Nayak KS, Kim EY, Ye JC. k-t FOCUSS: a general compressed sensing framework for high resolution dynamic MRI. *Magn Res Med* 2009;61:103–116.
13. Gamper U, Boesiger P, Kozerke S. Compressed sensing in dynamic MRI. *Magn Res Med* 2008;59:365–373.
14. Donoho DL. Compressed sensing. *IEEE Trans Informat Theory* 2006;52:1289–1306.
15. Le Gall D. MPEG: a video compression standard for multimedia applications. *Communications ACM* 1991;34:46–58.
16. Candes E, Romberg J, Tao T. Robust uncertainty principles: exact signal reconstruction from highly incomplete frequency information. *IEEE Trans Informat Theory* 2006;52:489–509.
17. Renxiang L, Bing Z, Liou M. A new three step search algorithm for block motion estimation. *IEEE Trans Circuits Syst Video Technol* 1994;4:438–442.
18. Po L, Ma W. A novel four-step search algorithm for fast block motion estimation. *IEEE Trans Circuits Syst Video Technol* 1996;6:313–317.
19. Zhu S, Ma K. A new diamond search algorithm for fast block-matching motion estimation. *IEEE Trans Image Proc* 2000;9:287–290.
20. Nie Y, Ma K. Adaptive rood pattern search for fast block-matching motion estimation. *IEEE Trans Image Proc* 2002;11:1442–1449.
21. Axel L, Dougherty L. MR imaging of motion with spatial modulation of magnetization. *Radiology* 1989;171:841–845.
22. O'Sullivan J. A fast sinc function gridding algorithm for Fourier inversion in computer tomography. *IEEE Trans Med Imaging* 1985;4:200–207.
23. Sedarat H, Nishimura D. On the optimality of the gridding reconstruction algorithm. *IEEE Trans Med Imaging* 2000;19:306–317.
24. Moriguchi H, Duerk J. Modified block uniform resampling (BURS) algorithm using truncated singular value decomposition: fast accurate gridding with noise and artifact reduction. *Magn Res Med* 2001;46:1189–1201.
25. Rosenfeld D. New approach to gridding using regularization and estimation theory. *Magn Reson Med* 2002;48:193–202.
26. Dale B, Wendt M, Duerk J. A rapid look-up table method for reconstructing MR images from arbitrary k-space trajectories. *IEEE Trans Med Imaging* 2001;20:207–217.
27. Liang Z, Lauterbur P. An efficient method for dynamic magnetic resonance imaging. *IEEE Trans Med Imaging* 1994;13:677–686.